qualitativereseachjournal.com
Vol. 25 / No. 04 / 2025
ISSN: 1468-7941

Optimizing Hydraulic Fracturing Techniques for Horizontal Well Applications in Enhanced Geothermal Systems

Khosraw Ubaidy[*1], Cheng Linsong[2]

[*1,2]*Oil and Gas Field Development Engineering Department, The Unconventional Oil and Gas Research Institute, China University of Petroleum-Beijing, 18 Fuxue Road, Changping, Beijing 102249, China*

[*1]Khosraw_ubidy@yahoo.com

DOI: https://doi.org/10.5281/zenodo.17364583

ABSTRACT

Geothermal energy is a renewable energy source that can be found in abundance on our planet. Only a small fraction of it is currently converted to electrical power, though in recent years installed geothermal capacity has increased considerably all over the world. In this research, we assumed a model for designing of Enhanced Geothermal System, EGS. We used Computer-Modeling Group, CMG reservoir simulation software to create the typical Hot Dry Rock, HDR reservoir. Two wells one injection of cold water and one production of hot water are installed in the model with three different surface water injection rates. There are some hydraulic fractures are created by the mentioned software. Three different hydraulic fracturing half-length are assumed. The different fracturing half-length and surface water injection rate considered in order to evaluate the sufficient energy production. As a result, the energy production rate, thermal breakthrough and hot water production rate are defined. The aforementioned results are illustrated by some graphs, charts and tables. In this research the production of energy is quantified in a period of 10 years.

Keywords: Hot dry rock (HDR); Enhance Geothermal System (EGS); Geothermal energy; Hydraulic fracturing; CMG

INTRODUCTION

Enhanced geothermal systems (EGS) refer to methods of harvesting energy from Earth's crust by passing fluid through a zone of enhanced permeability in rock at depth. The enhancements come from drilling to sufficient depths that high temperatures are reached; creating enough permeability that fluid can be flushed at significant rates through the hot rock deep in the crust, the objective being to transfer the thermal energy to the fluid without excessive loss of fluid into the rock; and extracting the energy from the fluid to produce useful effects, either in terms of electricity generation or heating operations Fig. 1.

Increasing the supply of local and renewable energy has become a central issue across society, which highlights the necessity to re-evaluate all alternative energy sources [1]. Geothermal energy is a low-carbon and recyclable renewable energy, with the features of large reserves, wide distribution and

environmental friendliness. Compared to hydro-thermal geothermal resources, most of the geothermal energy is stored in hot crystalline rocks with no or little fluid in a depth range of about 3 to 10 km, at a temperature between 150 and 650 ℃ [2]. This is often called hot dry rock (HDR).

The Enhanced Geothermal System (EGS) represents the key technology of the HDR heat development project, with a research history of more than 40 years [3]. It requires water to be circulated from injection well to production well, via an artificial thermal reservoir constructed by hydraulic fracturing [4]. In this paper, we assumed a model for designing of Enhanced Geothermal System, EGS. We used Computer-Modeling Group,

CMG reservoir simulation software to create the typical Hot Dry Rock, HDR reservoir. Two wells one injection of cold water and one production of hot water are installed in the model with three different surface water injection rates. There are some hydraulic fractures are created by the mentioned software. Three different hydraulic fracturing half-length are assumed. The different fracturing half-length and surface water injection rate considered in order to evaluate the sufficient energy production. As a result, the energy production rate, thermal breakthrough and hot water production rate are defined. The aforementioned results are illustrated by some graphs, charts and tables. In this research the production of energy is quantified in a period of 10 years. For EGS, the primary role of hydraulic fracturing is to establish a satisfactory fracture network between a production well and an injection well. Hydraulic fracturing has already been a valuable technique in several industries to stimulate reservoir rock, with the objective varying from increased oil and gas recovery in the petroleum business to establishing a circulation network in geothermal industry. There are, however, two main goals of fracturing that are common across industries. The first is to reach the desired volume of rock, and the second to ensure satisfactory connectivity within the fracture network. These two goals can at times be difficult to achieve, and doing so is an important challenge to better the understanding of how untouched rock mass behaves to stimulation. Hydraulic fracturing can be simplified into a process that happens when the fluid pressure at a given point in earth exceeds the least of the principal stresses [7].

qualitativereseachjournal.com
Vol. 25 / No. 04 / 2025
ISSN: 1468-7941

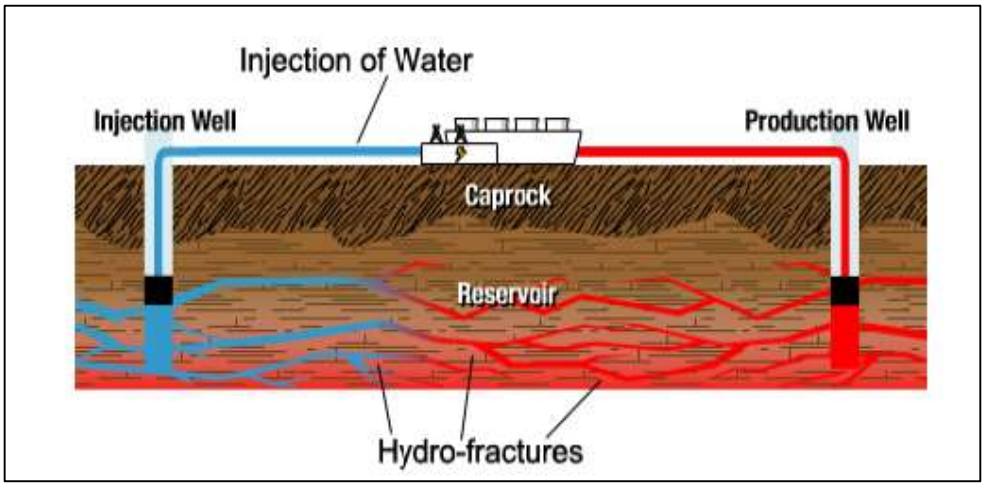

Figure 1. A typical HDR reservoir with an injection and production well.

MATERIALS AND METHODS

A fractured reservoir may contain millions of connected discrete fractures of limited length and millions of matrix blocks of finite dimensions and shapes. This fractured reservoir may be idealized by assuming linear or radial fluid flow in the network of uniform-aperture fractures, and a mixture of matrix blocks with regular shapes and different sizes in a representative elementary volume (REV) of the fractured medium. In this case, novel analytical solutions were developed to couple global heat convection - conduction in fractures with heat conduction in the rock matrix [3].

A conceptual geothermal reservoir, consisting of an injection and production well doublet in a homogenous porous media, is considered (Figure 1). The geothermal reservoir performance is described by two factors: the thermal performance of the reservoir (the time for thermal breakthrough at the production well), and the pressure profile in the reservoir (the pressure drive required to maintain a desired flow rate between the injection and production wells). As we know the EGS is a two-phase two-component reservoir. The two phases are liquid and gas (vapor) phases, while the two components are air and water components.

Each of the two components can exist in either of the two phases. Basically, the governing equations are build based on the mass conservation of components, and the flux term is calculated from phase flow by Darcy's law. In EGS the governing equations of mass and heat flow are both in general conservation form, as follows:

$$\frac{dM^k}{dt} = \nabla.\vec{F}^K + q^k \qquad (1)$$

qualitativeresearchjournal.com
Vol. 25 / No. 04 / 2025
ISSN: 1468-7941

In the above equation, k refers to mass component or heat. In our simulator, by integrating the above equation on a representative element volume (REV), we can get the following integrated governing equation:

$$\frac{d}{dt}\int_{v_n} M^k dV_n = \int_{\Gamma_n} \vec{F}^k . \vec{n} d\Gamma_n + \int_{V_n} q^k dV_n \tag{2}$$

In the above equation, n is the normal vector on the surface Γn, pointing inward to the REV. On the left side of the above equation, the accumulation term of the fluid equation is

$$M^k = \phi \sum_{\beta} S_\beta \rho_\beta X_\beta^k \tag{3}$$

The accumulation term of heat equation can be written in a similar way as follows

$$M^k = (1-\phi)\rho_R C_R T + \phi \sum_{\beta} S_\beta \rho_\beta u_\beta \tag{4}$$

The accumulation of heat contains two terms. The first term (1 − ∅) is the energy stored by rock while the second term is the energy stored by fluid. On the right side of Equation (2-1), the mass flux of liquids consists of advection and diffusion, as shown in Equation (2-5)

qualitativeresearchjournal.com
Vol. 25 / No. 04 / 2025
ISSN: 1468-7941

$$\vec{F}^{k}_{k} = \vec{F}^{k}_{k_{adv}} + \vec{F}^{k}_{k_{dis}} \tag{5}$$

The advective flux of a component is the sum over all phases:

$$\vec{F}^{k} = \sum_{\beta} X^{k}_{\beta} \vec{F}_{\beta} \tag{6}$$

where $\vec{F}_{\beta}$ is given by the multiphase version of Darcy's law;

$$\vec{F}_{\beta} = -K \frac{K_{r\beta}\rho_{\beta}}{\mu_{\beta}} (\nabla P_{\beta} - \rho_{\beta} g) \tag{7}$$

The diffusive mass flux is given by

$$\vec{F}^{K} dif = -\phi \tau_{0} \sum_{\beta} \tau_{\beta} \rho_{\beta} d^{K}_{\beta} \nabla X^{k}_{\beta} \tag{8}$$

Where the tortuosity τ_0 is an intrinsic property of rock matrix while the tortuosity τ_β is a property of the fluid . d^{k}_{β} is the molecular diffusion co efficient for component k in phase β. The heat flow includes conduction and convection

$$\vec{F}^{k=3} = -\left[(1-\phi) K_{R} + \phi \sum_{\beta} S_{\beta} K_{\beta} \right] \nabla T + \sum_{\beta} h_{\beta} \vec{F}_{\beta} \tag{9}$$

qualitativereseachjournal.com
Vol. 25 / No. 04 / 2025
ISSN: 1468-7941

Where k_R and K_β are properties of the rock and the liquid respectively and $\vec{F}_\beta$ is the liquid flow term from Equation.

The time for thermal breakthrough in the reservoir (i.e., for the temperature of the produced fluid to drop below the initial reservoir temperature, T_o) is defined as the life-time of the well doublet, Δt, and is described by Eq. (2-10) in Gringarten (1978):

$$\Delta t = \left[\emptyset + (1-\emptyset)\frac{\rho_r C_r}{\rho_w C_w}\right]\frac{\pi}{3}\frac{D^2 h}{Q} \quad (10)$$

In the equation 2-10, D is the distance between wells in m, Q is the volumetric injection/production well flow rate (m^3/s), h is the reservoir thickness (m), $\emptyset$ is the reservoir porosity, $\rho_w C_w$ is the water heat capacity ($kJ/m^3/C^o$), and $\rho_r C_r$ is the rock heat capacity ($kJ/m^3/C^o$).

The pressure drive between the wells in the reservoir, Δp, (or more accurately, the difference between the injection and production well pressure), is described by Gringarten (1978), Eq. (13)) as the pressure drawdown in the production well. Muskat (1946) describes how to relate the pressure difference between the wells. The result is:

$$\Delta p = \frac{\mu Q}{\pi k h} 1n\left(\frac{D}{r_{well}}\right) \quad (11)$$

where Δp is the pressure difference between injection and production wells, k is the reservoir permeability, μ is the water viscosity, and r_{well} is the well radius [3].

RESERVOIR SIMULATION

We used computer modeling group, CMG – IMEX, reservoir simulation software to create the typical Hydrothermal Dry Rock, HDR reservoir Fig. 2. with the idea to generate hydraulic fractures and thermal energy. The IMEX model converted to STARS in order to reproduce the effects of heat transfer and quantify the amount of energy produced from the reservoir. The reservoir model is designed using an orthogonal corner point grid with a resolution of 20 (I-direction) × 10 (J-direction) × 10 (K-direction) meters, with ten layers. The areal grid size of 500×100 meters were verified to have an acceptable approximation to the solution of an analytic model. It is assumed that the reservoir permeability is equal in all directions (I, J and K) within each grid block. The thermal properties of water i.e., heat capacity and thermal conductivity are constant. The properties of HDR reservoir and water used in this study are shown in table 1.

qualitativereseachjournal.com
Vol. 25 / No. 04 / 2025
ISSN: 1468-7941

Table 1. Data of reservoir and water used in CMG numerical analysis

Number	Properties	Data
1	Porosity	0.01%
2	Permeability	0.01mD
3	Rock compressibility (CPOR)	1.2E-5
4	Reference pressure box (PRPOR)	20000 kpa
5	Reservoir temperature	160 °C
6	Injection temperature	86 °C
7	Generate data up to max pressure	35000 kpa
8	Bubble point	5000 kpa
9	Gas density	0.85
10	Reference pressure for water properties	20000 kpa
11	Water salinity (ppm)	1000
12	Pressure	20000 kpa
13	Reference Depth	2250
14	Constant Bubble point pressure	5000 kpa
15	DTWELL	1e-4
16	DTMIN	1e-6
17	NCUT	15

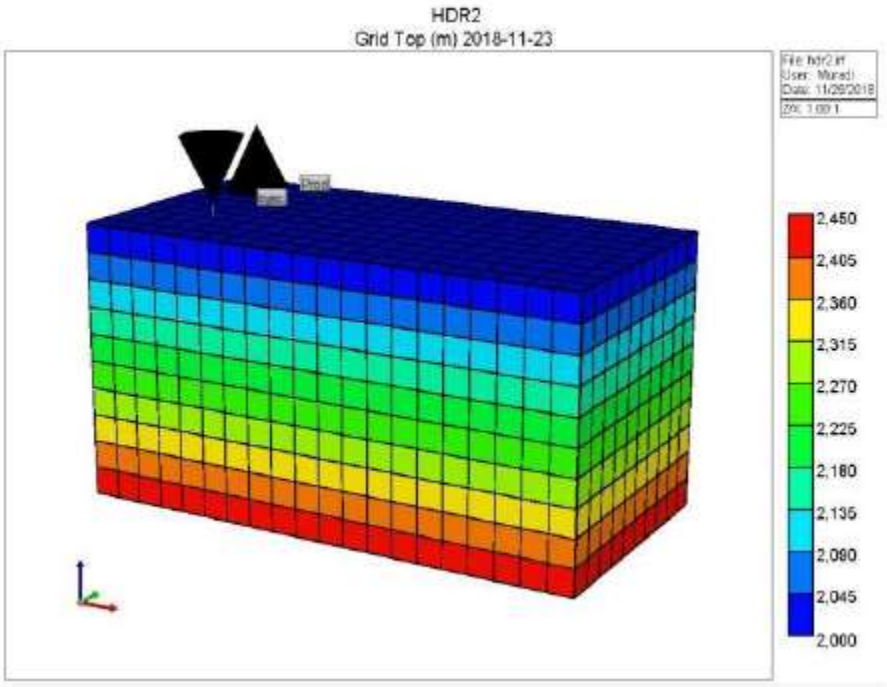

Figure 2. Typical HDR reservoir model created 152 by CMG.

The initial reservoir temperature is 160 ℃ and water injection temperature is 80 ℃. The maximum injection well bottom hole pressure of 35,300 kPa was used as a well constraint, to maintain injection pressure below the typical fracture gradient (0.60 psi/ft). The minimum production well bottom hole pressure was set to 21,300 kPa, to prevent produced hot water from flashing into vapor. Two wells are included in the model, one injector of cold water and one producer of hot water, the energy produced will be quantified in a period of 10 years. In this paper Three different hydraulic fracturing half-length 100m, 150m and 200m with three different surface water injection rates are assumed, Fig. 2. The surface water injection rates are constant and it is $50m^3$/day, $100m^3$/day and $150m^3$/day. The data shown in table 1, is used in CMG calculation.

In this study we create a set of relative permeability curves (figure 4) in order to mimic the flow of cold and hot water. Table 1 are parameters for the analytical relative permeability curves. The relative permeability data is taken from CMG tutorial. This HDR reservoirs commonly is tight and the wells require hydraulic fracturing to inject and produce the water. The Hydraulically Fractured Wells wizard performs Local Grid Refinement to bring the grid-block size close to the actual fracture width, to model the fracture more explicitly than using the skin factor. Fig. 3-4 shows the hydraulic fractures are created in order to inject cold water and produce hot water. The properties of hydraulic fracturing are used in this study is shown in table 2. Fig. 3 shows the flow from injection well to production well through the fractures made by CMG numerical simulation. Fig. 5a shows the water saturation in the reservoir and the cold-water flow from the injection well to the production well. Fig. 5b shows the reservoir temperature which is 160c and heat flow that transferred by water to the production well.

qualitativereseachjournal.com
Vol. 25 / No. 04 / 2025
ISSN: 1468-7941

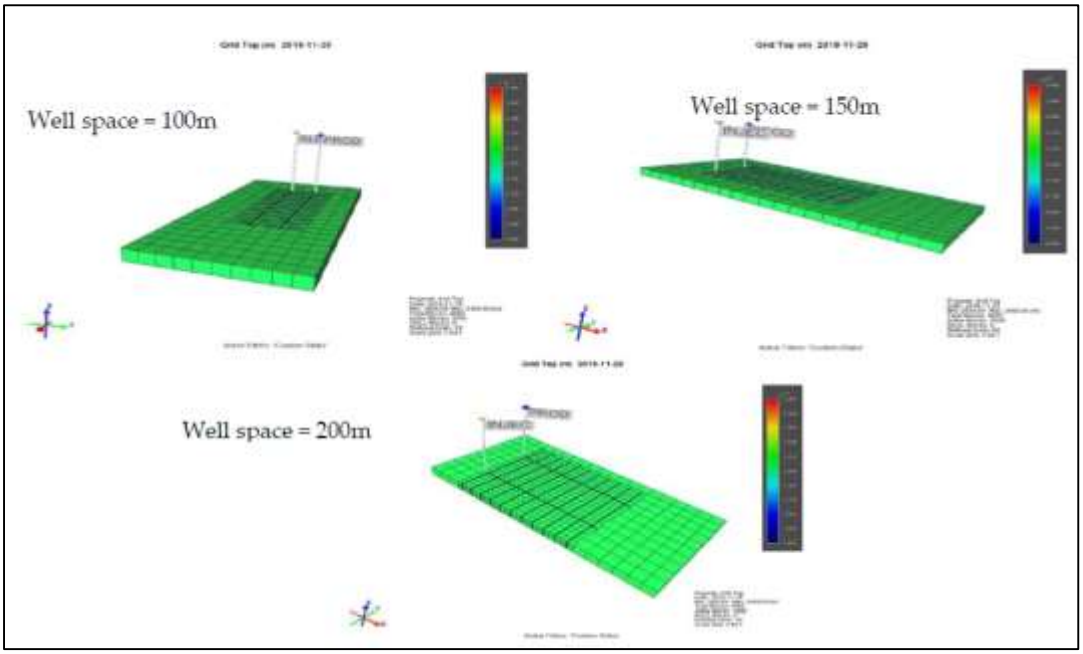

Figure 3. HDR reservoir model with different 179 hydraulic fracture half-length distance

qualitativeresearchjournal.com
Vol. 25 / No. 04 / 2025
ISSN: 1468-7941

Table 2. Parameters used for relative permeability curves.

Properties	Water
SWCON	0.10
SWCRIT	0.15
SOIRW	0.4
SORW	0.4
SOIRG	0.2
SORG	0.2
SGCON	0.05
SGCRIT	0.05
KROCW	0.8
KRWIRO	0.4
KRGCL	0.00
KROGCG	0.8

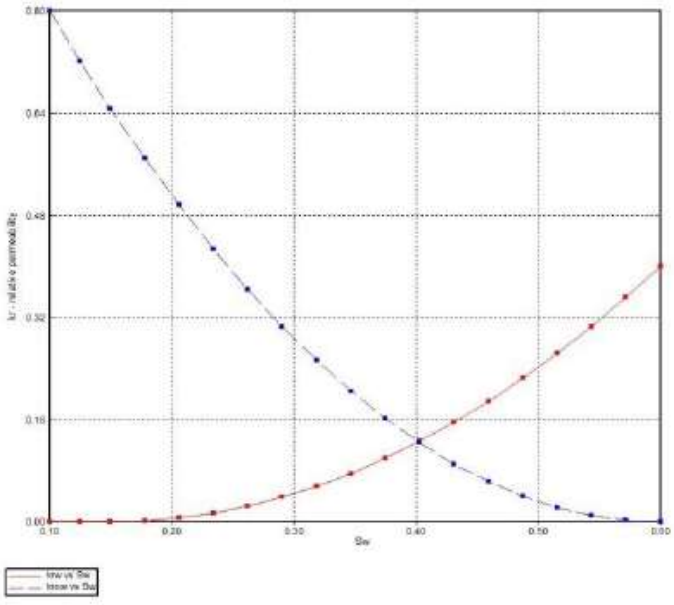

qualitativeresearchjournal.com
Vol. 25 / No. 04 / 2025
ISSN: 1468-7941

Figure 4. Relative permeability curves.

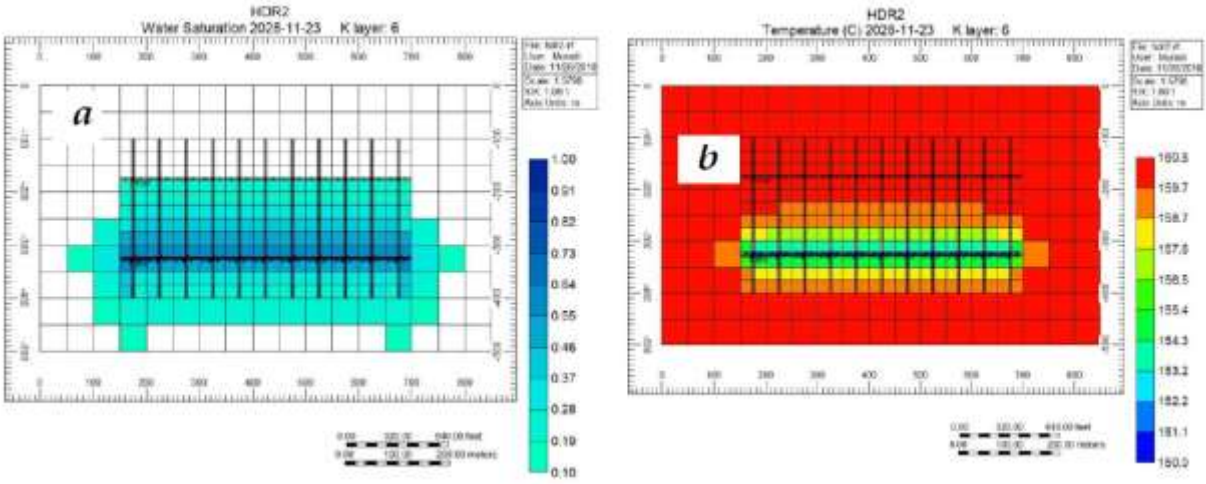

Figure 5. a) Water produced b) Thermal energy 185 produced comes from the injector well

RESULTS AND DISCUSSION

In order to model the conditions of a hot dry rock with negligible amounts of fluids, the model is initialized with immobile water and gas with low mobility according with the relative permeability curve defined in Fig. 4. Here are the aforementioned three models with different surface water pumping rate and fracturing half length. Through the CMG – Star the energy production and thermal breakthrough are evaluated as follows:

HDR MODEL WITH WELL DISTANCE OF 100M

In this reservoir the hydraulic half-length is designed to be 50m. Three different surface water injection rate 50m^3/day, 100m^3/day and 150m^3/day are pumped in to the reservoir. Fig. 6 shows the injection and production of water. It seems from the figure, when the pumping rate is 50 m^3/day the production rate in the 4th years is 25m^3/day however at the 10th years, which is the last year of operation, it is 42m^3/day. When the pumping rate is 100m^3/day the production rate in the 4th years of operation is 45m^3/day and at the 10th years it is 75m^3/day. When the pumping rate is 150m^3/day the production rate in the 4th years of operation is 76m^3/day and at the 10th years, which is the last year of the operation, it is 108m^3/day.

qualitativereseachjournal.com
Vol. 25 / No. 04 / 2025
ISSN: 1468-7941

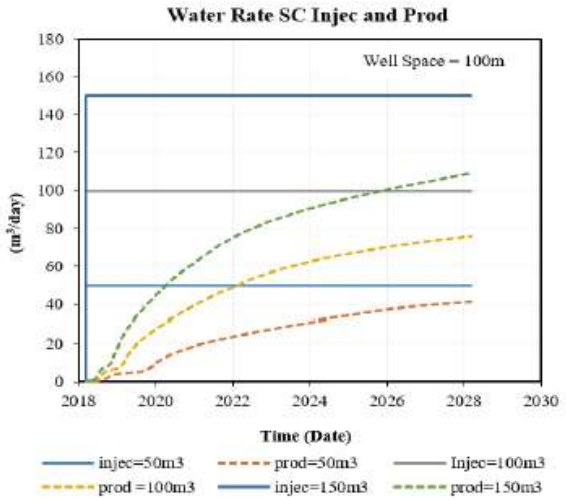

Figure 6. Injection and production rate of water

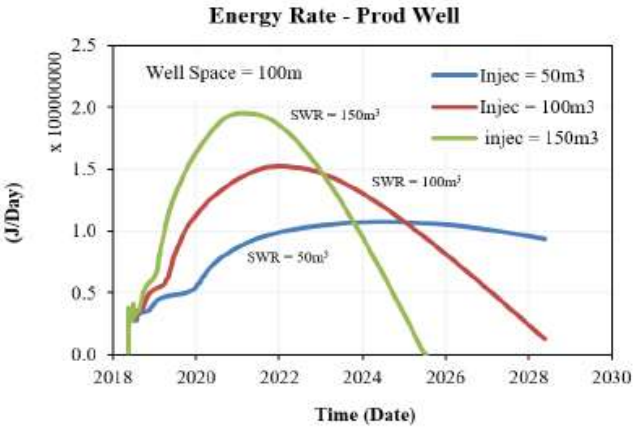

Figure 7. Energy rates from production well with different surface water pumping rate

Figure 7 shows the energy rate extracted from the production well with different injection pumping rate. It shows from the figure that the highest energy rate comes from injection pumping rate of 150m^3/day however the latter in years 7 and 8 there are no sufficient energy produces from the reservoir and the energy breakthrough accrues. There is some stable energy produced from pumping rate of 50m^3/day.

HDR MODEL WITH WELL DISTANCE OF 150M

In this reservoir, the well distance is designed to be 150m. Three different surface water injection rate 50m^3/day, 100m^3/day and 150m^3/day are conducted. The half-length of the fractures are assumed to be 75m. Fig. 3.8 shows the injection and production rate. As shows in the figure, When the pumping rate is 50 m^3/day the production rate seems stable and it is close to injection rate. When the pumping rate is 100 m^3/day the production rate in the 4th years of operation is 92m^3/day and at the 10th years is 96m^3/day. When the pumping rate is 150 m^3/day the production rate in the 4th years of operation is 128m^3/day and at the 10th years, which is the last year of operation, is 138m^3/day.

qualitativeresearchjournal.com
Vol. 25 / No. 04 / 2025
ISSN: 1468-7941

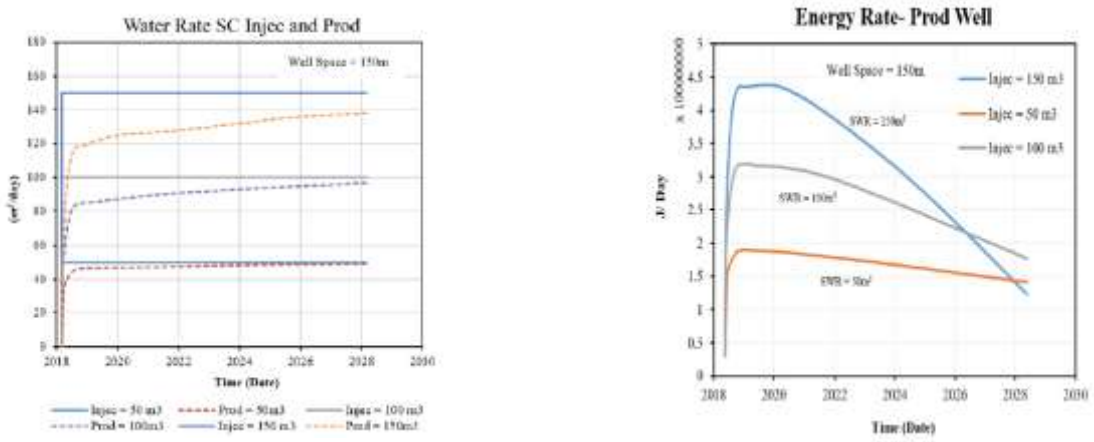

Figure 8. Energy rates from production

Figure 8 shows the energy rate extracted from the production. It shows from the figure that the highest energy rate comes from injection pumping rate of 150 m^3/day however the energy drops down soon. It seems from the figure that energy comes from pumping water rate of 100m^3/day and 50m^3/day is more stable but the energy is less than the pumping rate of 150 m^3/day.

HDR MODEL WITH WELL DISTANCE OF 200M

In this reservoir the well distance is designed to be 200m. Three different surface water injection rate 50 m3/day, 100m3/day and 150m3/day of cold water are pumped into the reservoir. The half-length of the fractures are assumed to be 100m. It seems from Fig. 9, when the pumping rate is 50 m3/day the production rate in the 4th years is 21 m3/day however at the 10th years, which is the last year of operation, is 48m3/day. When the pumping rate is 100 m3/day the production rate in the 4th years of operation is 50m3/day and at the 10th years is 88m3/day. When the pumping rate is 150m3/day the production rate in the 4th years of operation is 79m3/day and at the 10th years, which is last year of operation, is 120m3/day.

Figure 10 shows the energy rate extracted from the production well with different injection pumping rate. It shows from the figure that the highest energy rate comes from injection pumping rate of 150m3/day and the energy is getting high rate in the next years. It seems from the figure that energies come from pumping rate of 100 and 50m3/day are getting high but the energy is less than the pumping rate of 150m3/day.

qualitativereseachjournal.com
Vol. 25 / No. 04 / 2025
ISSN: 1468-7941

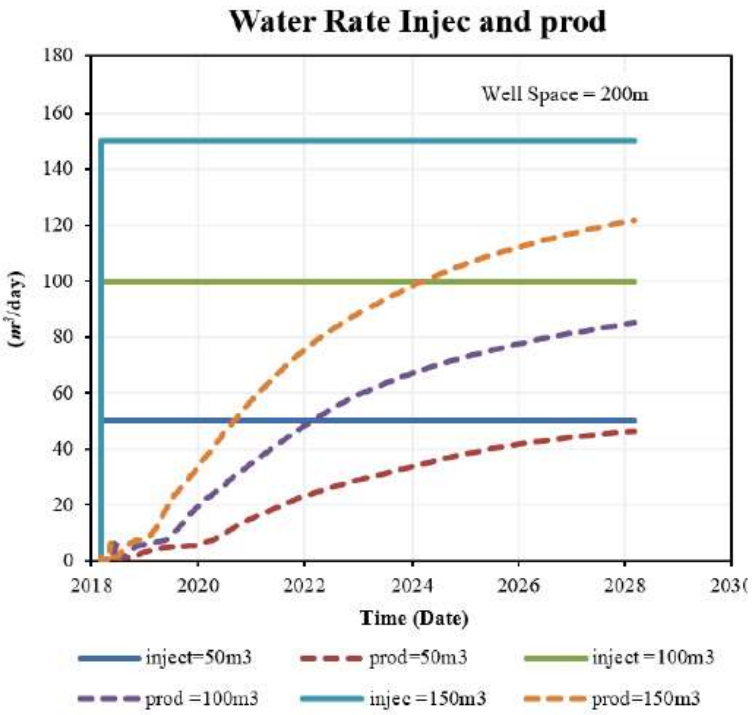

Figure 9. Injection and production rate of water

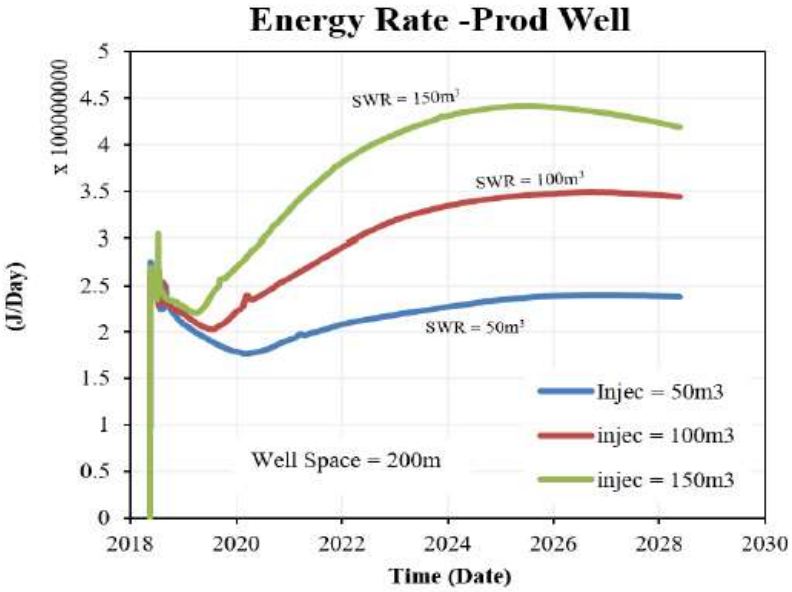

Figure 10. Energy rates from production

CONCLUSIONS

The Enhance Geothermal System, EGS is studied by designing a typical HDR reservoir through CMG reservoir simulation software. The generating of hydraulic fractures in the HDR reservoir, surface water injection and success of hot water thermal energy are analyzed. The main conclusions are obtained from this research is as follows:

1. A typical HDR reservoir with low porosity and permeability created in computer modeling group (CMG-IMEX) with the idea to generate hydraulic fractures. The IMEX model converted to STARS in order to reproduce the effects of heat transfer and quantify the amount of energy produced from the reservoir.

2. Two wells are included in the model, one surface water injector and one producer of hot water. The different fracturing half-length and surface water injection rate considered in order to evaluate the sufficient energy production. the energy produced will be quantified in a period of 10 years.

3. The results show that the gas produced from the HDR is negligible and the water production comes from the injector well as it is expected due to the presence of hydraulic fractures generated in these two wells. and can be observed that as more water is injected the energy produced is became less.

Acknowledgments: This research was supported by: JSPS KAKENHI Grant Number JP21K04959 and Akita University Support for Fostering Research Project.

Conflicts of Interest: The authors declare no conflict of interest.

REFERENCES

1. Alsaba, M.T., Al Dushaishi, M.F. & Abbas, A.K. A comprehensive review of nanoparticles applications in the oil and gas indus-268 try. J Petrol Explor Prod Technol 10, 1389–1399 (2020). https://doi.org/10.1007/s13202-019-00825-z
2. Hogeweg AS, Hincapie RE, Foedisch H, Ganzer L (2018) Evaluation of aluminium oxide and titanium dioxide nanoparticles for 270 EOR applications. In: SPE Europec featured at 80th EAGE conference and exhibition, 11–14 June, Copenhagen, Denmark. https://doi.org/10.2118/190872-MS
3. Ogolo, N. A., Olafuyi, O. A., and M. O. Onyekonwu. "Enhanced Oil Recovery Using Nanoparticles." Paper presented at the SPE Saudi Arabia Section Technical Symposium and Exhibition, Al-Khobar, Saudi Arabia, April 2012. Doi: https://doi.org/10.2118/160847-MS
4. Ajulibe, Daniel, Ogolo, Naomi , and Sunday Ikiensikimama. "Viability of SiO2 Nanoparticles for Enhanced Oil Recovery in the Niger Delta: A Comparative Analysis." Paper presented at the SPE Nigeria Annual International Conference and Exhibition, Lagos, Nigeria, August 2018. doi: https://doi.org/10.2118/193423-MS
5. Iravani, M., Khalilnezhad, Z. & Khalilnezhad, A. A review on application of nanoparticles for EOR purposes: history and current challenges. J Petrol Explor Prod Technol (2023). https://doi.org/10.1007/s13202-022-01606-x
6. Tinuola H. Udoh, Improved insight on the application of nanoparticles in enhanced oil recovery process, Scientific African, Volume 13, 2021, e00873, ISSN 2468-2276, https://doi.org/10.1016/j.sciaf.2021.e00873.
7. Samarshi Chakraborty, Pradipta Kumar Panigrahi, Stability of nanofluid: A review, Applied Thermal Engineering, Volume 174, 2020, 115259, ISSN 1359-4311, https://doi.org/10.1016/j.applthermaleng.2020.115259.
8. Ilyas, S.U., Pendyala, R., Marneni, N. (2017). Stability of Nanofluids. In: Korada, V., Hisham B Hamid, N. (eds) Engineering Applications of Nanotechnology. Topics in Mining, Metallurgy and Materials Engineering. Springer, Cham. https://doi.org/10.1007/978-3-319-29761-3_1
9. Derkani MH, Fletcher AJ, Fedorov M, Abdallah W, Sauerer B, Anderson J, Zhang ZJ. Mechanisms of Surface Charge Modification of Carbonates in Aqueous Electrolyte Solutions. Colloids and Interfaces. 2019; 3(4):62. https://doi.org/10.3390/colloids3040062
10. Kasprzyk-Hordern B. Chemistry of alumina, reactions in aqueous solution and its application in water treatment. Adv Colloid Interface Sci. 2004 Jun 30;110(1-2):19-48. doi: 10.1016/j.cis.2004.02.002. PMID: 15142822.
11. Hendraningrat, Luky & Li, Shidong & Torsæter, Ole. (2013). A Coreflood Investigation of Nanofluid Enhanced Oil Recovery in Low-Medium Permeability Berea Sandstone. Soc. Pet. Eng.. 2. 10.2118/164106-MS.
12. Amin Keykhosravi, Pavel Bedrikovetsky, Mohammad Simjoo, Experimental insight into the silica nanoparticle transport in dolomite rocks: Spotlight on DLVO theory and permeability impairment, Journal of Petroleum Science and Engineering, Volume 209, 2022, 109830, ISSN 0920-4105, https://doi.org/10.1016/j.petrol.2021.109830.
13. Odo Jude Emeka, Onyejekwe Ifeanyi, Anthony Chikwe, Angela Nwachukwu, Okereke Ndubuisi, Oguamah Ifeanyi, Obikaonu Agnes Chidiebere. Effect of the Application of Aluminium Oxide on

Recovery in Enhanced Oil Recovery. Engineering and Applied Sciences. Vol. 6, No. 2, 2021, pp. 41-48. doi: 10.11648/j.eas.20210602.12

14. Peng, C., Crawshaw, J. P., Maitland, G. C., Martin Trusler, J., & Vega-Maza, D. (2013). The pH of CO2-saturated water at temperatures between 308K and 423K at pressures up to 15MPa. The Journal of Supercritical Fluids, 82, 129–137. https://doi.org/10.1016/j.supflu.2013.07.001
15. Derkani MH, Fletcher AJ, Abdallah W, Sauerer B, Anderson J, Zhang ZJ. Low Salinity Waterflooding in Carbonate Reservoirs: 304 Review of Interfacial Mechanisms. Colloids and Interfaces. 2018; 2(2):20. https://doi.org/10.3390/colloids2020020
16. Anh V. Nguyen, Geoffrey M. Evans, Graeme J. Jameson, (2015), Electrical Double-Layer Interaction between Spherical Particles, in: Somasundaran, P., Namita Deo, Raymond Farinato, Vicki Grassian, Max Lu, Martin Malmsten, K.L. Mittal, Ramanathan Nagarajan, Patra Partha, Gleb Sukhorukov and Darsh Wasan, Encyclopedia of Surface and Colloid Science, Third Edition, Boca Raton: CRC Press, 27 Aug 2015, DOI: 10.1081/E-ESCS3-120000598
17. Esfandyari Bayat, A., Junin, R., Shamshirband, S. et al. Transport and retention of engineered Al2O3, TiO2 and SiO2 nanoparticles through various sedimentary rocks. Sci Rep 5, 14264 (2015). https://doi.org/10.1038/srep14264
18. Khilar, K. C., & Fogler, S. H. (2013). Migrations of Fines in Porous Media (Theory and Applications of Transport in Porous Media Book 12) (1998th ed.). Springer.
19. E. Lennart Sjöberg, David T. Rickard, Calcite dissolution kinetics: Surface speciation and the origin of the variable pH dependence, Chemical Geology, Volume 42, Issues 1–4, 1984, Pages 119-136, ISSN 0009-2541, https://doi.org/10.1016/0009-315 2541(84)90009-3.
20. Bayat, A.E., Junin, R., Ghadikolaei, F.D. et al. Transport and aggregation of Al2O3 nanoparticles through saturated limestone under high ionic strength conditions: measurements and mechanisms. J Nanopart Res 16, 2747 (2014). https://doi.org/10.1007/s11051-014-2747-x
21. Berner, R. (1975). The role of magnesium in the crystal growth of calcite and aragonite from sea water. Geochimica Et Cosmo-chimica Acta, 39(4), 489–504. https://doi.org/10.1016/0016-7037(75)90102-7